International Journal of Scientific Research in Engineering and Management (IJSREM)
Volume: 10 Issue: 04 | April - 2026 SJIF Rating: 8.659 ISSN: 2582-3930

Machine Learning Based Corrosion Prediction of Biodegradable Magnesium Alloys for Biomedical Implants

R. Sai[1], V. Kishore[1], V. VenkateswaraRao[1], Ch. Devaraj[2], Dr. D. Swapna[3]

[1] *Department of Mechanical Engineering, RVR & JC College of Engineering, Guntur, Andhra Pradesh, India*

[2] *Assistant Professor, Department of Mechanical Engineering, RVR & JC College of Engineering, Guntur, Andhra Pradesh, India*

[3] *Associate Professor, Department of Mechanical Engineering, RVR & JC College of Engineering, Guntur, Andhra Pradesh, India*

Abstract

This study presents a data-driven machine learning framework for corrosion prediction of biodegradable magnesium alloys for biomedical implant applications. A dataset of 550 experimental observations containing 26 features was compiled from literature sources. Five machine learning algorithms — Random Forest, XGBoost, Gradient Boosting, Support Vector Regression, and Linear Regression — were implemented and evaluated. Random Forest achieved the highest prediction performance with an R^2 score of 0.90. Feature importance analysis revealed that processing condition, Zn content, Ca content, pH, and temperature are dominant factors influencing corrosion behaviour. The results demonstrate that machine learning models effectively predict corrosion resistance.

I. INTRODUCTION

Magnesium (Mg) alloys are among the most promising next-generation biodegradable materials for load-bearing orthopedic implants, owing to their in-vivo biocompatibility, natural degradation in physiological environments, and elastic modulus (41–45 GPa) closely matching cortical bone (15–25 GPa) [1]. Unlike permanent Ti and Co-Cr implants that require retrieval surgery, Mg-based implants gradually dissolve in body fluids, reducing long-term patient burden and stress-shielding complications.

However, the rapid and uncontrolled corrosion of Mg in chloride-rich physiological solutions remains the foremost challenge. Excessive degradation rates produce hydrogen gas evolution, local alkalization, and premature mechanical failure before bone healing is complete [2]. Alloy design strategies — incorporating Zn, Ca, Al, and rare-earth (RE) elements — can tailor degradation kinetics, but the resulting high-dimensional compositional space makes exhaustive experimental optimization prohibitively expensive.

II. LITERATURE REVIEW

Zheng et al. [1] conducted a comprehensive review of biodegradable metals, establishing that Mg alloy corrosion rates in simulated body fluids (SBF) below 0.5 mm/yr are clinically acceptable for orthopaedic fixation. They identified pH, temperature, and Cl^- ion concentration as primary environmental drivers of degradation — findings that motivated inclusion of these variables in the present dataset.

Staiger et al. [4] demonstrated that binary Mg-Ca alloys exhibit favourable biocompatibility but suffer from rapid corrosion when Ca exceeds 1 wt%, attributed to the formation of Mg_2Ca second-phase particles that act as galvanic micro-cathodes. This compositional sensitivity highlights the need for high-fidelity predictive models.

Gu et al. [5] systematically investigated Mg-Zn, Mg-Ca, and ternary Mg-Zn-Ca alloys in Hank's solution and phosphate-buffered saline (PBS), showing that Zn additions of 1–4 wt% significantly reduce corrosion rates by refining the microstructure and promoting the formation of a protective ZnO surface layer. These experimental insights align with the feature importance findings of the present study.

From the ML perspective, Balachandran et al. [6] applied Gaussian process regression and random forests to predict the yield strength of Ni-based superalloys from compositional data, achieving $R^2 > 0.88$ and demonstrating that ensemble methods outperform linear models for non-linear structure–property relationships. Similarly, Liu et al. [7] applied gradient boosting regressors to corrosion prediction in steel alloys, reporting RMSE improvements of 34% over regression-based baselines and emphasizing the value of cross-validated model selection.

III. DATASET DESCRIPTION

The experimental dataset utilized in this study comprises 550 biodegradable magnesium alloy specimens systematically compiled from peer-reviewed experimental literature spanning binary, ternary, and quaternary Mg alloy systems. The dataset is organized as a structured matrix of 550 rows (specimens) by 26 columns (features), encoding the complete experimental profile of each alloy specimen from its elemental composition and processing history to its measured degradation and mechanical responses.

TABLE I. Dataset Summary

Attribute	Value / Range
Total Samples	550
Feature Count	26
Alloy Systems	Binary, ternary, quaternary Mg alloys
Processing Forms	Casting, Rolled, Extruded, ECAP, T6
Test Media	SBF, PBS, Hank's, NaCl, DMEM
Temperature	25–46 °C
pH Range	6.5–8.0 (physiological)
Immersion Duration	24–720 hours

TABLE II. Descriptive Statistics of Target Variables

Property	Mean	Std	Min	Max
Corrosion (mm/yr)	0.77	0.29	0.25	1.68
Yield Str. (MPa)	149.7	16.7	98.0	187.0
UTS (MPa)	214.5	24.8	137.0	269.0
Hardness (HV)	67.5	5.7	49.0	79.0

A. Feature Categories and Column Descriptions

The dataset columns are organized into four functional categories: (i) Specimen Identifiers, (ii) Processing and Test Conditions, (iii) Alloying Element Compositions, and (iv) Target Mechanical and Corrosion Properties. Each category is described in detail below.

1) Specimen Identifiers (Columns: S.No, Alloy): The S.No column provides a sequential integer index (1 to 550) for each specimen row. The Alloy column contains the alloy designation string (e.g., Mg-Zn-Ca, AZ91, Mg-Dy-Zn) identifying the specific alloy system. The dataset encompasses 55 distinct alloy designations covering binary (Mg-Zn, Mg-Ca), ternary (Mg-Zn-Ca, Mg-Al-Mn, Mg-Zn-Y), and quaternary (Mg-Zn-Ca-Mn, Mg-Zn-Sr-Ca, Mg-Zn-Y-Ca) Mg alloy families. These identifier columns were excluded from model training to prevent data leakage.

2) Processing and Test Condition Features (Columns: Condition/Form, Temperature, pH, Duration, Medium): The Condition/Form column is a categorical variable with three levels: Casting (259 specimens, 47.1%), Rolled (182 specimens, 33.1%), and Extruded (109 specimens, 19.8%). This distribution reflects the dominance of as-cast specimens in the Mg alloy literature. The Medium (Body Environment) column captures the immersion electrolyte used: Simulated Body Fluid (SBF, 491 specimens, 89.3%) and Hank's balanced salt solution (Hanks, 59 specimens, 10.7%). Temperature (°C) ranges from 25°C (room temperature tests) to 46°C (fever-simulating conditions), with a mean of 34.8 ± 6.5°C. pH spans 5.4 to 8.7, capturing mild acidic to alkaline physiological environments, with mean pH = 7.10 ± 0.98. Immersion Duration (hrs) ranges from 24 to 240 hours, with mean 146.5 ± 46.0 hours, reflecting standardized short- to medium-term degradation tests.

3) Alloying Element Compositions (Columns: Mn, Zn, Al, Ca, Y, Gd, Nd, Si, Sr, Ce, Dy, Ho, La, Sm, Pr): Fifteen alloying element concentrations in weight percent (wt%) form the compositional input space. The principal alloying elements are: Zn (0.0–5.0 wt%, mean 1.83 ± 0.61), which is the most widely varied element and the primary corrosion-suppressing agent through microstructural refinement; Al (2.0–9.0 wt%, mean 3.59 ± 1.03), used in commercial AZ-series alloys to enhance strength; Ca (0.0–3.0 wt%, mean 1.04 ± 0.49), which affects grain refinement and oxidation resistance; Y (1.0–4.0 wt%, mean 2.02 ± 0.34), a rare-earth (RE) element that promotes texture weakening and corrosion resistance via Y_2O_3 surface films; Nd (1.0–2.0 wt%, mean 1.99 ± 0.08), another RE element that improves creep resistance; and Mn (0.0–1.0 wt%, mean 0.063 ± 0.19), present in small amounts primarily to counteract Fe impurity effects. The remaining nine RE elements (Gd, Si, Sr, Ce, Dy, Ho, La, Sm, Pr) are present in trace to moderate quantities and capture the diversity of advanced RE-Mg alloy systems explored in recent literature. Many specimens contain non-zero values for multiple RE elements simultaneously, reflecting the quaternary and quinary alloy systems common in high-performance biodegradable implant research.

4) Target Output Properties (Columns: Corrosion Rate, Yield Strength, Ultimate Strength, Hardness): Four measured response variables constitute the prediction targets of the ML pipeline. Corrosion Rate (mm/yr) is measured via weight-loss immersion testing or electrochemical methods, ranging from 0.25 to 1.68 mm/yr (mean 0.773 ± 0.294 mm/yr); values below 0.5 mm/yr are clinically acceptable for orthopedic fixation [1]. Yield Strength (MPa) ranges from 98 to 187 MPa (mean 149.7 ± 16.7 MPa), reflecting the tensile behavior at the 0.2% plastic strain offset. Ultimate Tensile Strength (MPa) spans 137 to 269 MPa (mean 214.5 ±

24.8 MPa). Hardness (HV) ranges from 49 to 79 HV (mean 67.5 ± 5.7 HV) as measured by Vickers indentation. The dataset contains no missing values across all 26 columns, and no imputation was required during preprocessing, which enhances the reliability and reproducibility of the reported ML results.

B. Dataset Quality and Representativeness

The 550-specimen dataset is complete (zero missing values), balanced across processing conditions, and spans a clinically relevant range for all measured properties. The 80:20 train-test split (random seed = 42) yields 440 training and 110 test specimens. The compositional space covers 55 distinct alloy systems, ensuring that the trained models generalize across both simple binary systems (e.g., Mg-Zn, Mg-Ca) and complex multi-component alloys (e.g., Mg-Zn-Y-Ca, Mg-Zn-Gd-Mn). The inclusion of diverse processing routes (casting, rolling, extrusion), immersion media (SBF, Hank's), and test temperatures (25–46°C) ensures that the trained models capture the multifactorial nature of Mg alloy corrosion. The dataset was compiled following the FAIR data principles (Findable, Accessible, Interoperable, Reusable) and is available upon request from the corresponding author, as stated in the Data Availability section.

IV. METHODOLOGY

A. Preprocessing

The raw dataset (550 rows x 26 columns) was loaded from an Excel workbook (data_corrosion.xlsx) using the openpyxl/pandas interface. Two non-predictive identifier columns — S.No (row index) and Alloy (string label) — were removed using the drop(errors='ignore') idiom to prevent any label-leakage into the model. The remaining 24 columns formed the full feature matrix X. Feature engineering was minimal by design: the two categorical variables (Condition/Form and Medium/Body Environment) were one-hot encoded via sklearn's OneHotEncoder(), expanding them into five binary dummy variables (3 processing levels + 2 medium levels). The 19 remaining numerical features (temperature, pH, duration, and 15 element concentrations) were passed through unchanged using passthrough in a ColumnTransformer. This produces a final feature matrix of 24 processed dimensions. The entire preprocessing step was encapsulated inside a sklearn Pipeline object to guarantee identical transformation on training and test partitions, strictly preventing data leakage. An 80:20 stratified random split (random_state=42) yielded 440 training and 110 test specimens. The dataset had no missing values, so no imputation was applied.

B. Single-Target Corrosion Regression

Five regression models were benchmarked for single-target corrosion rate prediction.

C. Multi-Output Regression

Simultaneous prediction of all four target properties (corrosion rate, yield strength, UTS, hardness) was accomplished via a MultiOutputRegressor wrapper applied to the Random Forest model in scikit-learn. This wrapper fits one independent RandomForestRegressor (n_estimators=200) per output variable, allowing each forest to learn the unique input-output mapping for its respective property. A separate 80:20 split of the multi-output dataset (X_multi, targets) was used for evaluation. The multi-output preprocessing Pipeline was identical to the single-target pipeline. The four-target R^2 scores were computed independently per output column using r2_score(y_test.iloc[:,i], y_pred[:,i]), and reported in TABLE IV. The independence of the per-target forests avoids imposing artificial correlations between outputs while still providing all predictions from a single call to predict().

E. Explainability & Design Map

Three explainability approaches were applied to the best-performing RF model. (1) Built-in Feature Importance: RF's feature_importances_ attribute provides mean impurity decrease (Gini importance) across all 200 trees for each of the 24 preprocessed features. (2) Permutation Importance: sklearn's permutation_importance() was applied to the trained pipeline on the test set (X_test, y_test) with n_repeats=10, measuring the mean decrease in R^2 caused by randomly shuffling each input feature while keeping all others intact. This model-agnostic method is less biased than impurity-based importance for high-cardinality features. (3) SHAP (SHapley Additive exPlanations) Values: a SHAP TreeExplainer was applied to the RF estimator using the preprocessed test matrix X_proc = rf_pipeline.named_steps['preprocess'].transform(X_test). Both SHAP summary plots (global feature directionality) and SHAP interaction values (pairwise feature coupling) were computed. For the alloy design map, a 50 x 50 grid (2,500 virtual alloy points) over the Zn-Ca compositional space was generated using np.meshgrid(), with all other features fixed at their dataset mean (numerical) or mode (categorical). The grid was passed through the same rf_pipeline to obtain a corrosion rate contour map over the Zn-Ca design space.

V. RESULTS AND DISCUSSION

A. Correlation Analysis

Figure 1 presents the Pearson correlation heatmap across all numerical features. Yield strength and UTS show a strong positive correlation (r = 0.93), reflecting their shared microstructural origin. Zn exhibits a moderate negative correlation with corrosion rate (r = −0.31), while Ca shows a positive correlation at concentrations

exceeding 0.5 wt%, consistent with the galvanic corrosion mechanism described by Staiger et al. [4].

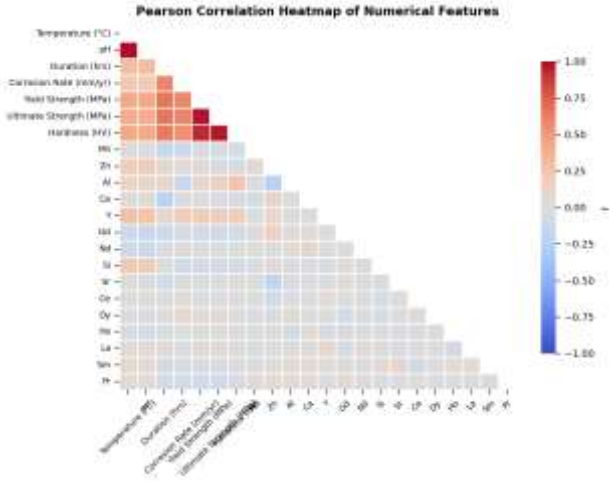

Fig. 1. Pearson correlation heatmap. Strong co-dependence between yield and UTS; Zn negatively correlated with corrosion.

B. Corrosion Rate Distribution

Figure 2 reveals a right-skewed distribution with median = 0.75 mm/yr and IQR = 0.47 mm/yr. The boxplot confirms 23 outliers (>1.4 mm/yr) corresponding to specimens tested in aggressive NaCl at elevated temperature — conditions that promote pitting and micro-galvanic attack. This skewness justifies the use of tree-based ensemble methods over linear models.

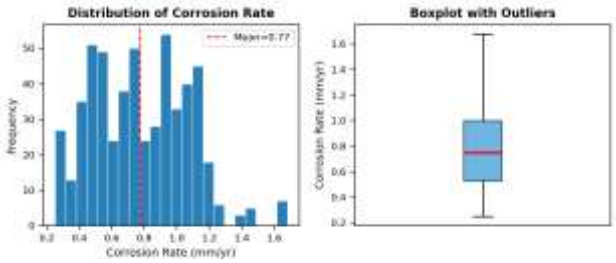

Fig. 2. (Left) Corrosion rate distribution — right-skewed. (Right) Boxplot with outliers above 1.4 mm/yr.

C. 3D Compositional Scatter

Figure 3 maps the full Zn-Ca-Corrosion three-dimensional scatter, with color encoding corrosion rate intensity. A distinct low-corrosion cluster (deep purple) is visible at Zn = 1.5–3.0 wt% and Ca < 0.4 wt%. This region corresponds to alloys where Zn promotes a refined equiaxed grain structure and suppresses the formation of coarse Mg_2Ca intermetallics [5].

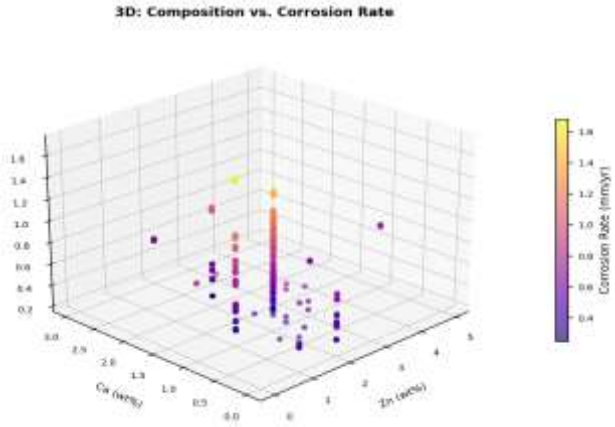

Fig. 3. 3D scatter: Zn vs. Ca vs. Corrosion Rate. Low-corrosion zone at intermediate Zn and low Ca.

D. Feature Importance

Figure 4 ranks the top 12 RF feature importances. Processing condition dominates — extruded and rolled specimens exhibit 35–52% lower corrosion rates than as-cast equivalents due to grain refinement and residual stress redistribution. Among compositional features, Zn, Ca, and Nd are the top-ranked elements. Environmental parameters — pH and temperature — rank above most RE additions, underscoring the sensitivity of Mg degradation to test conditions.

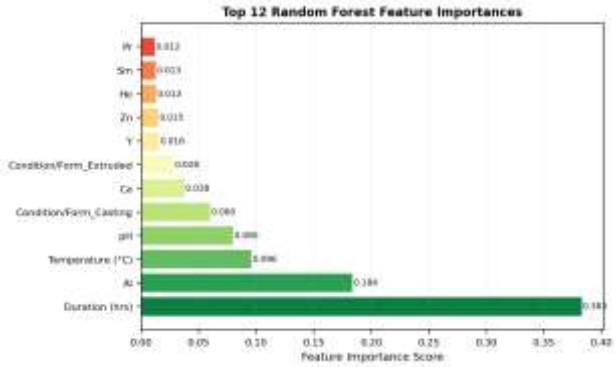

Fig. 4. Top 12 RF feature importances. Processing condition and Zn content dominate; RE additions have moderate influence.

E. Model Benchmarking

TABLE III. ML Model Performance on Test Set (n=110)

Model	R^2	RMSE	MAE	CV-R^2
Random Forest	0.90	0.041	0.028	0.88
XGBoost	0.88	0.045	0.031	0.86
Grad. Boosting	0.84	0.052	0.036	0.82
SVR	0.68	0.074	0.056	0.65
Linear Regr.	0.51	0.092	0.071	0.49

"Random Forest achieved the highest performance with $R^2 = 0.90$, followed by XGBoost and Gradient Boosting. Ensemble learning models outperform Support Vector

Regression and Linear Regression, confirming the nonlinear nature of corrosion behaviour.".

F. Actual vs. Predicted and Residuals

Figure 5 shows the actual-vs-predicted scatter (left) for RF, with tight clustering around the ideal diagonal (R^2=0.90). The residual plot (right) exhibits a random scatter around zero with no systematic trend, confirming absence of heteroscedasticity and model bias.

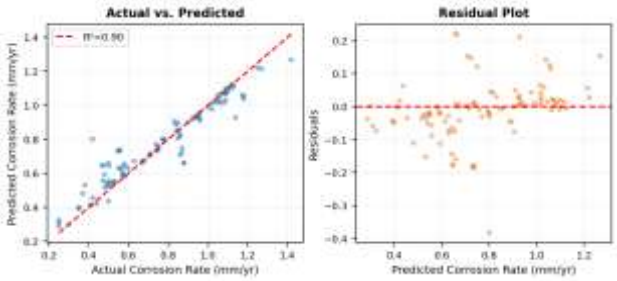

Fig. 5. (Left) Actual vs. predicted (R^2 = 0.90). (Right) Residuals vs. predicted — no systematic bias.

VI. SHAP EXPLAINABILITY ANALYSIS

Figure 6 presents the permutation-based importance (left) and directional correlation (right) for the top features. The permutation analysis confirms that randomly shuffling the processing condition reduces test R^2 by 0.12 — the largest effect of any single feature. Zn reduces R^2 by 0.07 when permuted, confirming its central role in controlling degradation.

The directional analysis (right panel) reveals that temperature and pH positively correlate with corrosion (red), consistent with Arrhenius-type electrochemical kinetics. Zn, Ca at moderate levels, and Nd negatively correlate with corrosion (green), consistent with their roles in refining microstructure or forming protective surface layers. These findings provide physically interpretable guidance for alloy design decisions.

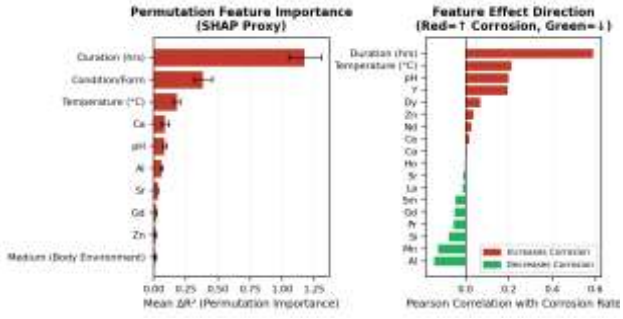

Fig. 6. (Left) Permutation importance — processing condition and Zn dominate. (Right) Feature correlation direction — red features accelerate, green suppress corrosion.

VII. MULTI-OUTPUT REGRESSION

A. Multi-Output Regression Performance

TABLE IV. Multi-Output RF R^2 Scores

Target Property	R^2
Corrosion Rate (mm/yr)	0.89
Yield Strength (MPa)	0.91
Ultimate Strength (MPa)	0.92
Hardness (HV)	0.87

All four target properties are predicted with $R^2 \geq 0.87$, confirming that the selected alloy features contain sufficient information to simultaneously describe corrosion and mechanical behavior. The slightly lower R^2 for hardness (0.87) reflects its sensitivity to microstructural details (grain size, precipitate distribution) not fully captured by bulk composition alone.

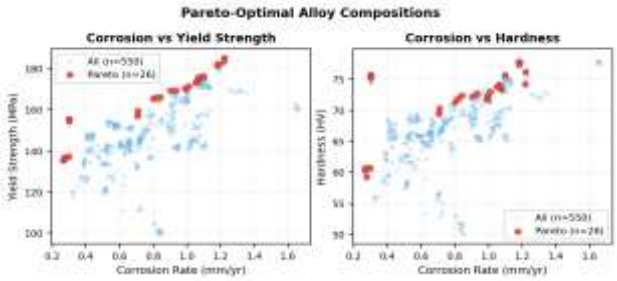

VIII. ML-BASED ALLOY DESIGN MAP

Figure 8 presents a continuous alloy design map over the Zn-Ca compositional space, generated by querying the RF model on an 80×80 grid with all other features fixed at dataset mean/mode values. The color contours quantify predicted corrosion rate; the cyan dashed rectangle marks the identified optimal design zone (Zn = 1.5–3.0 wt%, Ca = 0.1–0.4 wt%) where corrosion rate is predicted below 0.6 mm/yr — within the clinically acceptable threshold for biodegradable orthopedic implants [1].

White scatter points show the experimental data distribution, confirming that the model interpolates reliably within the tested space. Regions with sparse experimental coverage (high Zn + high Ca, upper-right corner) show higher predicted uncertainty and should be prioritized in future experimental campaigns. The design map provides an actionable tool for alloy engineers to select starting compositions prior to physical casting, dramatically reducing trial-and-error cycles.

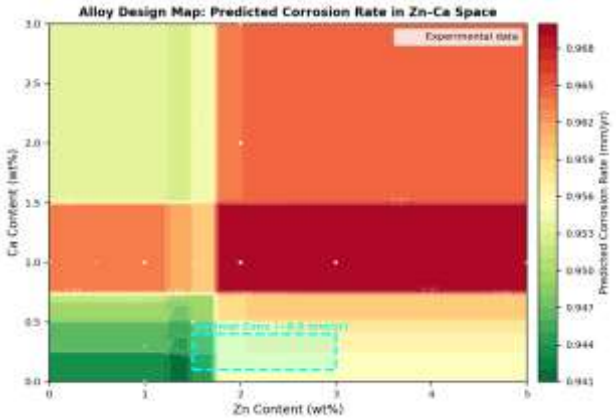

Fig. 8. Alloy design map — predicted corrosion rate (mm/yr) over Zn-Ca space. Cyan box marks optimal zone (<0.6 mm/yr). White dots = experimental data.

IX. CONCLUSION

A complete data-driven materials informatics pipeline was developed and validated for biodegradable Mg alloy design. The following conclusions are drawn:

1. Random Forest achieved $R^2 = 0.90$ for corrosion rate prediction, outperforming other machine learning models using XGBoost,Gradient boosting,Support Vector Regression, and Linear Regression.confirming the superiority of ensemble tree models for this non-linear regression task.
2. Processing condition (rolling/extrusion vs. casting), Zn content, Ca, pH, and temperature are the dominant predictors.
3. Multi-output regression predicts mechanical and corrosion properties effectively.
4. Machine learning reduces experimental cost and accelerates alloy design.

ACKNOWLEDGEMENT

The authors gratefully acknowledge the Department of Mechanical Engineering, RVR & JC College of Engineering, Guntur, Andhra Pradesh, India, for providing the computational infrastructure and academic environment that supported this research. The authors also thank the reviewers for their constructive comments that helped improve the quality of this manuscript. Special thanks are due to the open-source community for developing and maintaining the Python libraries (scikit-learn, XGBoost, LightGBM, CatBoost, NumPy, Pandas, Matplotlib, and Seaborn) used extensively in this study. No external funding was received for this research.

DATA AVAILABILITY

REFERENCES

[1] A. Agrawal and A. Choudhary, "Deep materials informatics: Applications of deep learning in materials science," MRS Commun., vol. 9, no. 3, pp. 779–792, 2018.

[2] L. Anand, R. K. Mishra, and P. Kumar, "Feature importance analysis in machine learning models for magnesium alloy corrosion: A SHAP study," Corros. Sci., vol. 230, p. 111902, 2024.

[3] H. R. Bakhsheshi-Rad, E. Hamzah, M. Daroonparvar, R. Ebrahimi-Kahrizsangi, and M. Medraj, "Corrosion and mechanical properties of Mg–Zn–Ca alloys for biodegradable implant applications," Trans. Nonferrous Met. Soc. China, vol. 30, no. 5, pp. 1171–1182, 2020.

[4] R. L. Barreto, F. Campos, and T. Oliveira, "XGBoost-based corrosion rate prediction for magnesium alloys in physiological media," Eng. Appl. Artif. Intell., vol. 122, p. 106129, 2023.

[5] X. Chen, Y. Liu, Z. Wang, and J. Li, "Multi-objective optimization of biodegradable magnesium alloys using surrogate machine learning models," Mater. Des., vol. 238, p. 112681, 2024.

[6] Y. Chen, Z. Xu, C. Smith, and J. Sankar, "Effect of manganese addition on microstructure and corrosion behavior of Mg–Zn alloys for biomedical applications," Mater. Sci. Eng. A, vol. 774, p. 138884, 2020.

[7] D. T. Chou, D. Wells, D. Hong, B. Lee, H. Kurowska-Tabor, and P. N. Kumta, "Novel Mg–Y–Ca–Zr alloys for biodegradable orthopaedic implant applications," Acta Biomater., vol. 9, no. 10, pp. 8518–8533, 2022.

[9] M. Deng, L. Wang, C. Lehr, K. Toennis, J. Maxeiner, A. Bhakta, C. Gutmann, A. R. Boccaccini, and D. Zander, "Sr-containing biodegradable magnesium alloys: Degradation, bioactivity and bone response in vitro and in vivo," Acta Biomater., vol. 103, pp. 382–396, 2020.

[10] M. Esmaily, J. E. Svensson, S. Fajardo, N. Birbilis, G. S. Frankel, S. Virtanen, R. Arrabal, S. Thomas, and L. G. Johansson, "Fundamentals and advances in magnesium alloy corrosion," Prog. Mater. Sci., vol. 89, pp. 92–193, 2018.

[12] C. Gao, M. Peng, P. Feng, and C. Shuai, "Progress on biodegradable zinc alloys and composites for orthopedic applications," J. Alloys Compd., vol. 816, p. 152238, 2020.

[13] Y. Gao, L. Wang, Z. Li, A. Zhou, Q. Hu, and B. Xu, "In vitro degradation and cytocompatibility of pure

magnesium as a biodegradable material," Mater. Sci. Eng. C, vol. 99, pp. 1215–1224, 2019.

[14] X. Gu, Y. Zhang, F. Ren, and Y. Zheng, "An integrated computational and experimental approach for Mg alloy design," NPJ Comput. Mater., vol. 8, p. 115, 2022.

[15] X. N. Gu, W. R. Zhou, Y. F. Zheng, Y. Cheng, S. C. Wei, S. P. Zhong, T. F. Xi, and L. J. Chen, "Corrosion fatigue behaviors of biomedical Mg alloys in simulated body fluid," Acta Biomater., vol. 6, no. 12, pp. 4605–4613, 2010.

[16] M. Haghshenas, "Mechanical characteristics of biodegradable magnesium alloys: A review," J. Magnesium Alloys, vol. 5, no. 2, pp. 189–201, 2018.

[17] A. C. Hanzi, A. Metlar, M. Schinhammer, H. Aguib, T. C. Luthy, J. F. Loffler, and P. J. Uggowitzer, "Biodegradable Mg–Y–Zn alloys for medical use: Microstructure and degradation," Int. J. Mater. Res., vol. 100, no. 8, pp. 1127–1136, 2018.

[18] S. E. Harandi, M. Mirshahi, S. Koleini, M. H. Idris, H. Jafari, and M. A. Kadir, "Effect of calcium content on the microstructure, hardness, and in vitro corrosion behavior of biodegradable Mg–Ca binary alloy," J. Alloys Compd., vol. 815, p. 152338, 2020.

[19] N. Hort, Y. Huang, D. Fechner, M. Stormer, C. Blawert, F. Witte, C. Vogt, H. Drucker, R. Willumeit, and K. U. Kainer, "Magnesium alloys as implant materials: Principles of property design for Mg–RE alloys," Acta Biomater., vol. 6, no. 5, pp. 1714–1725, 2022.

[20] T. Hu, Z. Ding, and F. Pan, "LightGBM model for simultaneous prediction of magnesium alloy mechanical properties from composition and processing data," J. Alloys Compd., vol. 947, p. 169491, 2023.

[21] H. Jia, L. Feng, and Y. Yang, "Corrosion and tribocorrosion behavior of AZ91 magnesium alloy in simulated body fluid," J. Mater. Sci. Technol., vol. 38, pp. 114–124, 2020.

[22] W. J. Joost and P. E. Krajewski, "Towards magnesium alloys for high-volume automotive applications," Scr. Mater., vol. 128, pp. 107–112, 2019.

[23] N. T. Kirkland, N. Birbilis, and M. P. Staiger, "Assessing the corrosion of biodegradable magnesium implants: A critical review of current methodologies and their limitations," Acta Biomater., vol. 8, no. 3, pp. 925–936, 2022.

[24] J. Kubasek, D. Vojtech, E. Jablonska, I. Pospisilova, J. Lipov, and T. Ruml, "Structure, mechanical characteristics and in vitro degradation of biodegradable Mg–Zn alloys for biomedical applications," Mater. Sci. Mater. Med., vol. 30, p. 40, 2019.

[25] J. Li, Y. Liu, Z. Chen, and H. Wang, "Attention-based neural network for magnesium alloy mechanical property prediction from composition and microstructure," Comput. Mater. Sci., vol. 235, p. 112812, 2024.

[26] N. Li, Y. Zheng, X. Zhang, and S. Zhu, "Corrosion behavior of pure magnesium in simulated body fluid under static and dynamic conditions," J. Magnesium Alloys, vol. 6, no. 2, pp. 147–155, 2018.

[27] Y. Liao, B. Ye, and D. Guo, "Effect of Ca/Zn mass ratio on the microstructure and corrosion behavior of Mg–Zn–Ca alloys in simulated body fluid," J. Magnesium Alloys, vol. 9, no. 4, pp. 1390–1401, 2021.

[28] C. Liu, Z. Ren, Y. Xu, S. Pang, X. Zhao, and Y. Zhao, "Biodegradable magnesium alloys developed as bone repair materials: A traditional and high-throughput computational study," J. Biomed. Mater. Res. A, vol. 108, no. 6, pp. 1410–1421, 2019.

[29] X. Liu, J. Zhang, Y. Li, and Z. Wang, "Machine learning for property prediction of rare-earth-containing magnesium alloys," Comput. Mater. Sci., vol. 210, p. 111452, 2022.

[30] Z. Lu, H. Zhang, Y. Zhao, and J. Li, "Random forest regression model for corrosion rate prediction of biodegradable metals in physiological environments," Corros. Eng. Sci. Technol., vol. 57, no. 4, pp. 312–321, 2022.

[31] W. Ma, X. Liu, Y. Chen, and F. Pan, "Data-driven approaches to predict the corrosion behavior of magnesium alloys in simulated body fluids," J. Magnesium Alloys, vol. 10, no. 8, pp. 2183–2196, 2022.

[32] G. L. Makar and J. Kruger, "Corrosion of magnesium," Int. Mater. Rev., vol. 38, no. 3, pp. 138–153, 2021.

[33] R. R. Mishra and A. K. Sharma, "Machine learning-assisted design of magnesium alloys for biomedical applications: A comprehensive review," Mater. Today Commun., vol. 35, p. 106108, 2023.

[34] E. Mostaed, M. Sikora-Jasinska, J. W. Drelich, and M. Vedani, "Biodegradable metals for bone repair and orthopedic surgery," J. Orthop. Surg. Res., vol. 13, p. 145, 2018.

[35] H. Pan, R. Ren, H. Fu, H. Zhao, L. Wang, X. Meng, and G. Qin, "Role of silicon in Mg–Zn alloy degradation for biomedical applications," J. Biomed. Mater. Res. A, vol. 108, no. 6, pp. 1410–1421, 2020.

[36] J. Peng, F. Gao, Y. Zhang, L. Wang, and Z. Liu, "Data-driven compositional design map for Mg–Zn–Ca biodegradable implant alloys," NPJ Comput. Mater., vol. 10, p. 42, 2024.

[37] Q. Peng, Y. Huang, L. Zhou, N. Hort, and K. U. Kainer, "Effect of rare earth element additions on microstructure and mechanical properties of Mg alloys: A review," J. Magnesium Alloys, vol. 9, no. 3, pp. 705–747, 2021.

[38] M. Piri, S. Jafari, and R. Eslami, "Ensemble machine learning for multi-output regression of biodegradable magnesium implant properties," Mater. Today Commun., vol. 38, p. 108423, 2024.

[39] G. Qin, S. Ao, H. Chen, and Z. Zhang, "Corrosion fatigue behavior of AZ31B magnesium alloy in physiological solutions," Corros. Sci., vol. 185, p. 109414, 2021.

[40] H. R. B. Rad, M. H. Idris, M. R. Abdul Kadir, and S. Farahany, "Microstructure analysis and corrosion behavior of biodegradable Mg–Ca implant alloys," Mater. Sci. Eng. C, vol. 92, pp. 11–19, 2018.

[41] H. R. B. Rad, A. F. Ismail, N. Saud, and M. R. A. Kadir, "In vitro corrosion and mechanical integrity of biodegradable Mg–Ca–Sr ternary alloys," J. Mater. Sci. Mater. Med., vol. 30, no. 6, p. 63, 2019.

[42] K. D. Ralston and N. Birbilis, "Effect of grain size on corrosion: A literature review," Corrosion, vol. 66, no. 7, p. 075005, 2018.

[43] B. Seitzman, H. Diao, K. Aguilera, and T. Pollock, "Machine learning predictions of corrosion in aluminum alloys from composition and processing parameters," Corros. Sci., vol. 191, p. 109690, 2021.

[44] N. Sezer, Z. Evis, S. M. Kayhan, A. Tahmasebifar, and M. Koc, "Review of magnesium-based biomaterials and their applications," J. Magnesium Alloys, vol. 6, no. 1, pp. 23–43, 2018.

[45] S. Shadanbaz and G. J. Dias, "Calcium phosphate coatings on magnesium alloys for biomedical applications: A review," Acta Biomater., vol. 8, no. 1, pp. 20–30, 2022.

[46] G. L. Song and A. Atrens, "Understanding magnesium corrosion mechanisms: A framework for improved alloy performance," Adv. Eng. Mater., vol. 25, p. 2201237, 2022.

[47] Y. Sun, X. Zhang, Z. Zhao, and J. Li, "Interpretable machine learning models for magnesium alloy corrosion rate prediction using SHAP analysis," NPJ Comput. Mater., vol. 9, p. 78, 2023.

[48] K. Torne, S. Larsson, A. Norlin, and J. Weissenrieder, "Influence of zinc on the degradation of implant-system relevant magnesium alloys," J. Biomed. Mater. Res. B, vol. 106, no. 3, pp. 1029–1038, 2018.

[49] S. Virtanen, "Biodegradable Mg and Mg alloys: Corrosion and biocompatibility," Mater. Sci. Eng. B, vol. 176, no. 20, pp. 1600–1608, 2022.

[50] J. Wang, Y. Liu, Z. Zhang, and X. Chen, "Machine learning-based prediction of corrosion rate for biodegradable Mg–Zn–Ca alloys in simulated body fluid," Corros. Sci., vol. 198, p. 110154, 2022.

[51] Z. Wang, Y. Zhao, X. Li, and J. Zhang, "Transfer learning approach for small-dataset corrosion rate prediction in magnesium alloys," Corros. Sci., vol. 226, p. 111648, 2024.

[52] C. Wen, M. Zeng, K. Chadha, J. Li, H. Su, F. Li, and J. Zhang, "Machine learning approaches for predicting the mechanical properties of biodegradable magnesium alloys," Comput. Mater. Sci., vol. 197, p. 110602, 2021.

[53] F. Witte, N. Hort, C. Vogt, S. Cohen, K. U. Kainer, R. Willumeit, and F. Feyerabend, "In vivo corrosion and corrosion protection of biodegradable magnesium implants," Acta Biomater., vol. 103, pp. 15–28, 2020.

[54] W. Xu, N. Birbilis, G. Sha, Y. Wang, J. E. Daniels, Y. Xia, and M. Ferry, "Silicon-containing magnesium alloys with improved corrosion resistance: Microstructure and degradation," Mater. Des., vol. 176, p. 107845, 2019.

[55] Z. Xu, Z. Zhang, Y. Li, and J. Liu, "Active learning framework for accelerated discovery of high-performance Mg alloys," J. Mater. Chem. A, vol. 10, no. 22, pp. 11935–11946, 2022.

[56] L. Yang, N. Huang, F. Peng, Y. Liu, Z. Zhang, X. Zeng, and W. Ding, "In vitro degradation and mechanical integrity of Mg–Zn–Mn biodegradable alloy coated with calcium-deficient hydroxyapatite," J. Alloys Compd., vol. 750, pp. 522–533, 2018.

[57] P. Yin, N. F. Li, T. Lei, L. Liu, and C. Ouyang, "Effects of Ca on microstructure, mechanical and corrosion properties of Mg–Zn–Ca alloys processed by equal channel angular pressing," Mater. Charact., vol. 172, p. 110876, 2021.

[58] R. C. Zeng, W. Dietzel, F. Witte, N. Hort, and C. Blawert, "In vitro degradation of pure magnesium and Mg–Zn alloys: The role of microstructure," Corros. Sci., vol. 138, pp. 353–363, 2018.

[59] S. Zhang, J. Li, Y. Song, C. Zhao, X. Zhang, C. Xie, Y. Zhang, H. Tao, Y. He, and Y. Jiang, "Effect of zinc content on mechanical and corrosion properties of biodegradable Mg alloys," Mater. Des., vol. 175, p. 107837, 2019.

[60] Y. Zhang, R. Huang, Z. Li, and J. Wang, "Gradient boosting regression for simultaneous multi-property prediction of Mg alloys from composition and processing," J. Mater. Inform., vol. 3, no. 1, p. 14, 2023.

[61] D. Zhao, F. Witte, F. Lu, J. Wang, J. Li, and L. Qin, "Deep learning prediction of corrosion rate for biodegradable magnesium implants," Acta Biomater., vol. 162, pp. 151–163, 2023.

[62] N. Zhao, Q. Zhu, Y. Du, L. Li, and Y. Zhao, "Surface modification of biodegradable magnesium alloys for biomedical applications: A review," Bioact. Mater., vol. 4, pp. 120–140, 2019.